RSC Advances




ROYAL SOCIETY OF CHEMISTRY

www.rsc.org/advances

## Graphical Abstract

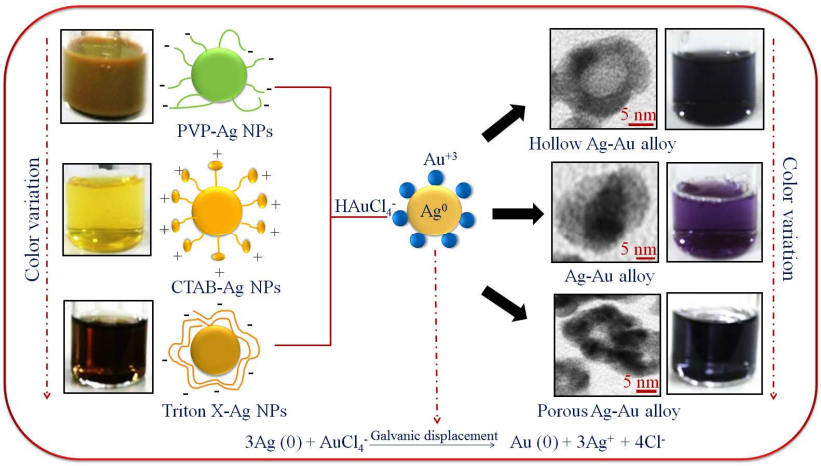


The surfactants like polyvinylpyrrolidone (PVP), cetyltrimethylammoniumbromide (CTAB) and Triton X-100 (TX) passivizing the surface of Ag nanoparticles (AgNPs) used as a template for deposition of Au, played an important role in controlling the morphology of resulting Ag-Au bimetallic nanostructures. This led to the formation of diverse morphologies i.e., hollow, solid and porous structures of Ag-Au bimetallic nanostructures which exhibited unique optical and surface properties, intense color variation and catalytic activity in comparison to monometallic AgNPs.

Journal Name

RSCPublishing

ARTICLE

# Morphological and physicochemical properties of Ag-Au binary nanocomposites prepared by different surfactants capped Ag nanoparticles

Cite this: DOI: 10.1039/xoxxoooooox

Received ooth January 2012,
Accepted ooth January 2012

DOI: 10.1039/xoxxoooooox

www.rsc.org/

Anila Monga and Bonamali Pal*

This paper demonstrates the influence of surfactants of different chemical nature passivizing the Ag nanoparticles (Ag NPs) on the morphology and physicochemical properties of Ag-Au bimetallic nanostructures. The Ag NPs were synthesized using: polyvinylpyrrolidone (PVP), cetyltrimethylammoniumbromide (CTAB) and Triton X-100 (TX), followed by the deposition of Au on their surface. TEM analysis revealed the formation of hollow Ag-Au shells (~15 nm) and mixed solid Ag-Au alloys (~20-25 nm) using PVP and CTAB-Ag NPs, respectively, as their reaction templates. In contrast, the porous-hollow aggregates of Ag-Au nanostructures (~16-22 nm) were evolved during the reaction between $Au^{3+}$ and TX-Ag NPs due to the difference in reaction rates between the $Au^{3+}$ ions and various surfactants capped Ag NPs. As a result, these diverse morphologies of bimetallic nanostructures exhibited a significant variation in surface plasmon (SP) band, color, hydrodynamic size and zeta potential as compared to their monometallic Ag NPs. For example, a SP band of PVP-Ag NPs (488 nm) gradually red-shifted to 550 nm with the addition of $Au^{3+}$ with notable color change from green to characteristic blue color indicating the composition change from Ag to Au rich. Therefore, the catalytic activity of various Ag-Au bimetallic nanostructures were found to be ~2 times higher than the monometallic Ag NPs for the reduction of different nitro-aromatic compounds attributed to the electronic effect at Ag-Au interface and their morphology.

**Keywords:** surfactant modified Ag nanoparticles; monometallic NPs; Ag-Au bimetallic nanocomposites; color variation; different morphologies; catalytic reduction; electronic effect

## 1. Introduction

Coinage metal (Au, Ag and Cu) nanoparticles (NPs) are of great interest due to their fascinating optical, electronic and catalytic properties in various types of chemical transformations,[1-4] such as hydrogenation of nitro-aromatic compounds, oxidation, carbon-carbon bond formation, etc. In comparison to Ag and Cu, Au NPs have been extensively studied because of their facile synthesis, homogeneity, high resistance to oxidation and tunable surface plasmon (SP) band in the visible region.[5-7] The Ag NPs also have the exceptional extinction coefficient than any metal that lead to its use as sensing agent and for antimicrobial treatment.[5,8-10] However, monometallic Ag NPs have been found to be of limited practical use because of its severe susceptibility to oxidation,[11-12] which makes the optical and catalytic results for these particles non-reproducible. An extensive number of capping agents such as polymers, ligands, dendrimers and surfactants have been used to enhance NPs suspension stability to prevent their aggregation through electrostatic repulsion, steric repulsion or both.[13] The mechanism and functional groups involved in colloid stabilization differs with the chemical structure of capping agents, which may lead to varying particle size and stability.[14] But these stabilizing agents block or hinder the true optical and catalytic properties to a certain extent.

Therefore, another helpful attempt has been employed to coat Ag NPs with a layer of Au which imparts chemical stability and protects the Ag core against oxidation due to the electron transfer[12,15,16] between two metallic elements. This gives rise to the formation of bimetallic nanocomposites (NCs) which exhibit unique superior activity, high selectivity, and stability, interesting electronic, optical, chemical, and biological properties as compared to their monometallic counterparts. This can be attributed to,[17-21] (i) the electronic effect, in which the electronic charge transfer takes place between two metal elements leading to a change in the electron density on the resultant bimetallic structures; (ii) synergistic effect, in which

each metal element in bimetallic NCs promote different elementary reaction steps. For example, the polyelectrolyte multilayer supported Au-Ag core-shell (k= 0.18 $min^{-1}$) NCs showed higher catalytic activity[22] for the reduction of *p*-nitrophenol to *p*-aminophenol by $NaBH_4$ than the corresponding monometallic Au (k=0.019 $min^{-1}$) and Ag (k=0.069 $min^{-1}$) nanospheres due to synergistic effect. The colloidal Ag NPs are known to serve as a versatile substrate or sacrificial templates for the material deposition (Au) or displacement reactions, respectively, leading to the formation of Ag-Au core-shell,[21,23-25] hollow,[26-29] cage-like,[30,31] porous[32] or alloyed[33] nanostructures. These different morphologies play an important role in catalysis where the hollow/porous NPs exhibit superior catalytic activities than their solid counterparts. For example, Xia et al. demonstrated that the Au nanocages and nanoboxes are better catalysts than solid Au NPs for a redox reaction.[31] The previous studies[30-32] showed that the replacement reaction between silver nanostructures and an aqueous $HAuCl_4$ solution can be used as a versatile method for generating metal nanostructures with hollow interiors. However, the role of capping agents, polymers, or surfactants adsorbing the Ag NPs (core) surface during these transformation reactions remain unexplored, as the coating of the shell-metal is a surface-driven charge transfer process. Therefore, the chemical species bound to the Ag NPs surface might alter the deposition rate of incoming metal, mechanism, and subsequently alloy formation. In the present study, we investigated the adsorbed surfactants on the Ag NPs surface, used during their synthesis can play a key role in the galvanic deposition mechanism. This chemical strategy allows to control the transformation of solid Ag NPs via the surface modification and presents the opportunity for the systematic study of optical, electro-kinetic parameters and catalytic properties of bimetallic NCs.

## 2. Experimental

### 2.1. Materials

Chloroauric acid ($HAuCl_4.3H_2O$), ascorbic acid ($C_6H_8O_6$), sodium hydroxide (NaOH), polyvinylpyrrolidone (PVP, $(C_6H_9NO)_n$), dimethyl formamide (DMF, $C_3H_7NO$), nitrobenzene ($C_6H_5NO_2$), 3-nitrotoluene ($C_7H_7NO_2$) and 1-chloro-3-nitrobenzene ($C_6H_4ClNO_2$) were obtained from Loba Chemie, India. Sodium borohydride ($NaBH_4$), trisodium citrate ($Na_3C_6H_5O_7$), Silver nitrate ($AgNO_3$), cetyltrimethylammoniumbromide (CTAB, $C_{19}H_{42}BrN$) and Triton X-100 (TX-100, $C_{14}H_{22}O(C_2H_4O)_n$) were purchased from Rankem, SDFCL, Fischer Scientific, Sigma Aldrich and Merck, India, respectively. All the chemicals were used as-received without any further purification. Deionized water was obtained using an ultra-filtration system (Milli-Q, Millipore) with a measured conductivity above 35 mho $cm^{-1}$ at 25 ˚C.

### 2.2. Preparation of Ag nanoparticles using different surfactants

The Ag NPs modified with different capping agents were prepared by using various surfactants viz., PVP, CTAB, and TX-100. An aqueous solution (10 mL) containing $AgNO_3$ (0.25 mM) and trisodium citrate (0.25 mM) followed by reduction with $NaBH_4$ (0.6 mL, 0.01 M) gave rise to the formation of Ag seeds.[34,35] This seed solution (ca. 0.0125 mL) was introduced at room temperature into the mixture of $AgNO_3$ (1 mL, 0.01 M), CTAB (10 mL, 80 mM), ascorbic acid (0.5 mL, 0.1 M) and NaOH (0.2 mL, 1M) resulting in the formation of CTAB-capped Ag NPs (CTAB-Ag NPs). The TX-100 capped Ag NPs (TX-Ag NPs) was prepared by the addition of above prepared seed solution (ca. 0.25 mL) at room temperature to the aqueous mixture containing TX-100 (25 mL, 0.015 M), $AgNO_3$ (1 mL, 0.01 M) and ascorbic acid (0.5 mL, 0.1 M) giving rise to brown color. On the other hand, the Ag NPs employing PVP (PVP-Ag NPs) were prepared through one-step seedless Solvo-thermal reduction route,[36,37] by refluxing $AgNO_3$ (0.0017 g) and PVP (42 mM) in DMF (20 mL) at 120 ˚C for 30 min in a round bottom flask yielding muddy-green color.

### 2.3. Preparation of Ag-Au bimetallic NCs

The Ag-Au bimetallic NCs were synthesized by taking pre-synthesized Ag NPs coated with different surfactants (demonstrated above). Each set of Ag NPs (0.8 mL) diluted with deionized water (4 mL) was treated with different amounts of $AuCl_4^-$ aqueous solution (15-35 µL, 0.01 M) for its deposition on the surface of Ag NPs. This resulted in the formation of Ag-Au NCs of different color depending on the amount of $Au^{3+}$ ions added.[38,39] The prepared bimetallic NCs were then washed with distilled water by centrifugation (8000 RPM for 5 min) and dispersed in 4 mL deionized water.

### 2.4. Characterization techniques

The optical properties of various Ag-Au bimetallic NCs were analyzed by UV-Vis absorption (Analytik Jena Specord-205) spectrophotometer and spectrofluorometer (Perkin-Elmer LS55) using xenon lamp as an excitation source. Transmission electron microscope (TEM) photographs and selected area diffraction pattern (SAED) were taken on the Hitachi 7500 model with resolution 2˚A operating at voltage 120 kV. The hydrodynamic size distribution of different NCs dispersed in water was determined by using Brookhaven 90 plus Particle Size Analyzer at 25 ˚C. It contains a 15 mW solid state laser operating at 635 nm and an avalanche photodiode detector. The scattered light was detected at an angle of 90˚. The zeta potential (ζ) was studied by taking 1.5 mL of NCs solution in a cuvette consisting of the palladium electrode mounted on a machined support using Brookhaven zeta plus at 25 ˚C.

### 2.5. Catalytic activity

The catalytic activity of various Ag-Au NCs relative to monometallic Ag NPs were evaluated for the reduction of (5 mL, 0.2 mM) nitrobenzene (NB), 3-nitrotoluene (NT) and 1-chloro-3-nitrobenzene (CNB) containing 100 µL ice-cold $NaBH_4$ solution (0.01 M) and calculated amounts of different NCs ($5.99 \times 10^{16}$ atoms) under similar conditions. The reaction



 

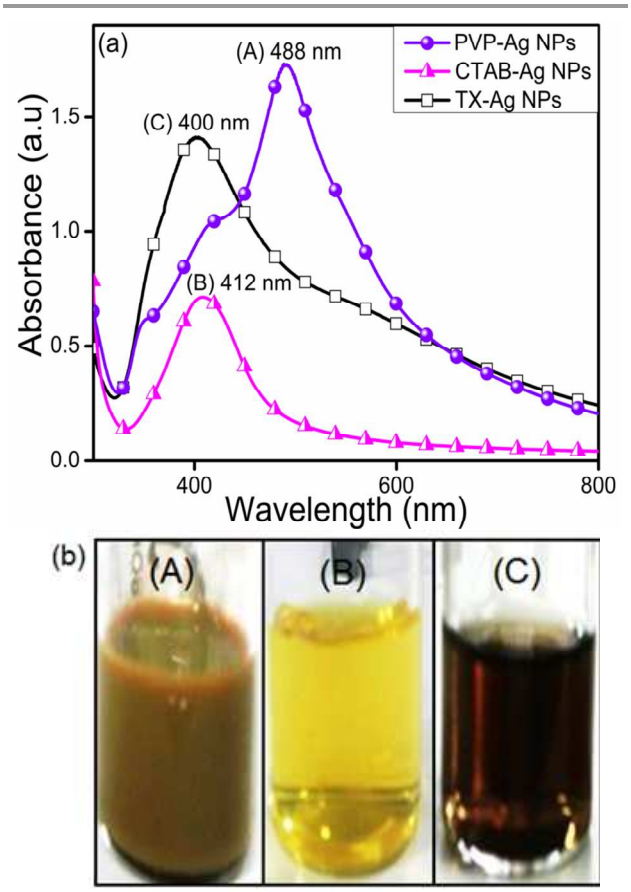


**Fig. 1.** Surface plasmon absorption spectra of (a) various Ag nanoparticles capped with different surfactants, and (b) their corresponding colors.

samples were analyzed by UV–Vis spectrophotometer ($\lambda_{max.}$ of NB ~270 nm, NT ~272 nm and CNB ~265 nm). The products were further quantified by HPLC-Agilent 1120 compact LC equipped with a Qualisil BDS C-18 column (250 × 4.6 mm, 5 µm) at λ = 254 nm with a flow rate of 1 mL/min and the eluent consisted of 70 % methanol and 30 % water solution.

## 3. Results and Discussions

### 3.1. Optical properties

The absorption studies revealed an intense surface plasmon (SP) band at maximum wavelength, 488 nm and a sharp SP band at 412 nm (Fig. 1a) corresponding to PVP-Ag NPs and CTAB-Ag NPs, respectively. On the other hand, TX-Ag NPs showed a blue-shifted and broader absorption peak at 400 nm as depicted in Fig. 1a. This suggested the formation of different sizes of Ag NPs of spherical shape as the plasmon frequencies are highly dependent on the morphology of NPs[40] and as a result, the Ag NPs capped with various surfactants exhibited different colors as seen in Fig. 1b. The optical properties of Ag NPs can be facilely adjusted by adding $Au^{3+}$ ions of varying amounts (15-35 µL, 0.01 M) and the atomic ratio for their deposition on the surface of Ag NPs is calculated to be 0.2-0.4 (Electronic supplementary information (ESI), Table S1). Fig. 2a shows that the SP band intensity of PVP-Ag NPs (488 nm) gradually decreased and became broader with a peak position red-shifted to, 500 nm and 592 nm through the addition of aqueous solution of $HAuCl_4^-$ ions (15-25 µL), which further broadened and decreased by an increased amount of $Au^{3+}$ ions (35 µL). These observations are consistent with the report[35] where the hollow Ag-Au NCs were obtained via replacement of Ag by Au. In the progressive galvanic replacement reaction, Au is deposited on the NPs surface with the Ag consumption from the core and it gave rise to the formation of hollow particles resulting in a red-shift[41] in the SP band of hollow Ag-Au NCs. This morphological change was further supported by the color change from green to red to light purple and blue as shown in Fig. 2b.

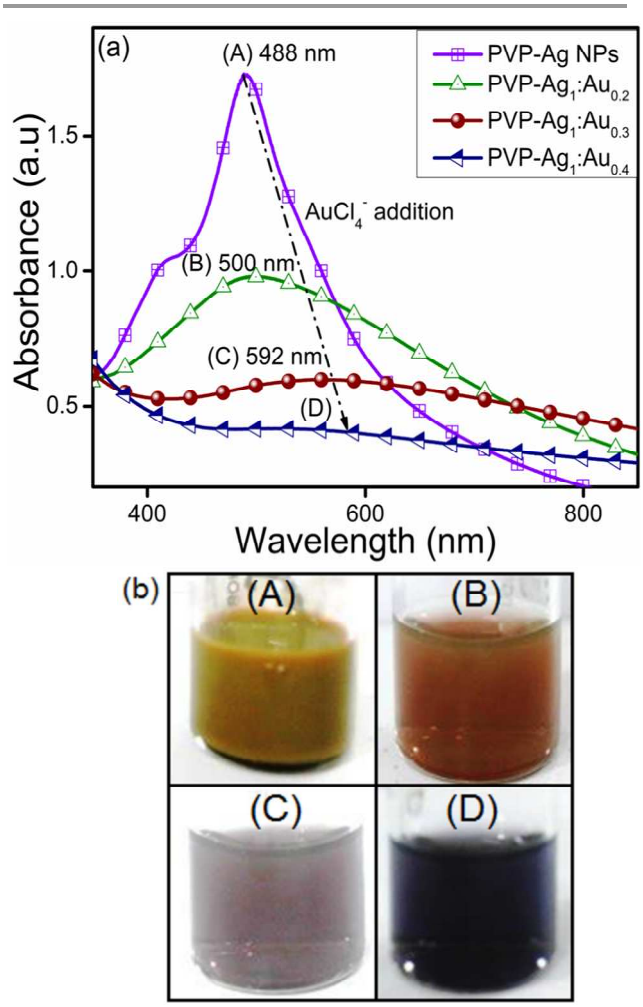


**Fig. 2.** Effect of different amounts (15-35 µL) of $HAuCl_4.3H_2O$ (0.01 M) deposition onto PVP-Ag nanoparticles for the (a) variation in the surface plasmon band, and (b) their respective color changes.

The SP band of CTAB-Ag NPs (412 nm) red-shifted to a broad peak at 546 nm of decreased intensity upon addition of $Au^{3+}$ ions (15 µL) accompanied by the color change from yellow to light blue (Fig. 3). However, with the higher addition of $Au^{3+}$ ions (25-35 µL), the intensity of absorption band

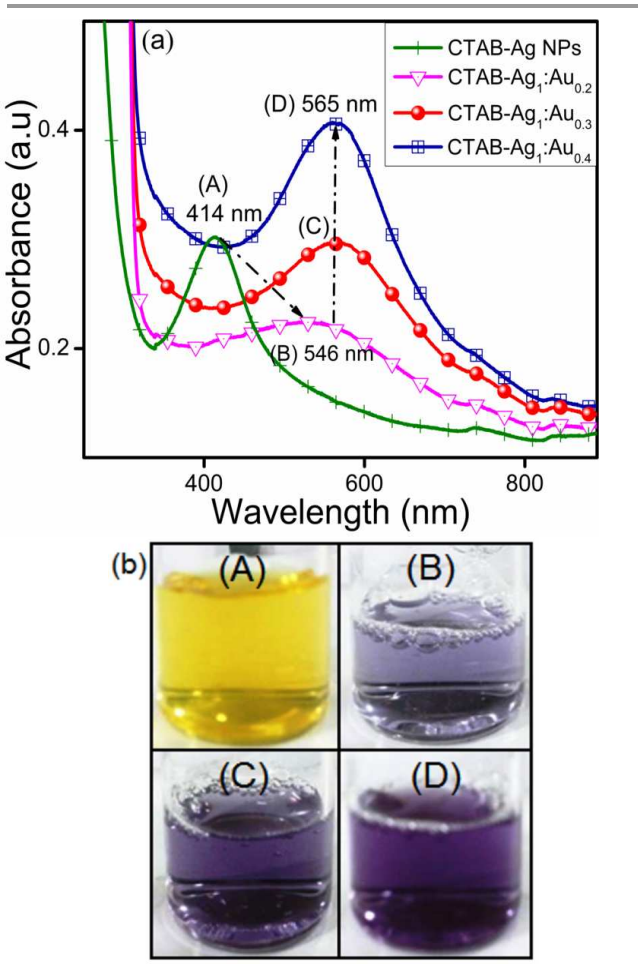


**Fig. 3.** Influence of different amounts (15-35 μL) of $HAuCl_4.3H_2O$ (0.01 M) deposition onto CTAB-Ag nanoparticles for the (a) variation in the surface plasmon band, and (b) their respective color changes.

corresponding to 565 nm increased, exhibiting a purple color solution. In case of the TX-Ag NPs, the characteristic SP band at 400 nm red-shifted in the range of 411 nm to 500 nm (Fig. 4a) of almost the same intensity after $Au^{3+}$ deposition (15-35 μL) along with a notable color change as shown in Fig. 4b. The red shifting in absorption peaks of Ag NPs with comparatively higher intensity and the color change from yellow/brown to light blue and finally to intense blue during the reaction process indicated the composition change of CTAB-Ag NPs or TX-Ag NPs from Ag to Au rich. These SP band variations in CTAB-Ag NPs and TX-Ag NPs were not similar to the observations in PVP-Ag NPs suggesting probably the formation of solid Ag-Au in the alloy structure form rather than the hollow interiors.

### 3.2. Electro-kinetic parameters

The observed red-shifts in the SP bands as noted in Fig. 2-4 is attributed to, (i) the changing dielectric function and composition of resulting alloy, and (ii) an increase in NCs size due to the deposition of Au on the Ag NPs surface[42] which can be measured by DLS particle size distribution. It showed that the average hydrodynamic size of PVP-Ag NPs (27 nm) displayed a gradual increase in particle sizes from 34 to 69 nm (Fig. 5a) after the deposition of Au on the surface of Ag NPs. Similarly, the hydrodynamic size of CTAB-Ag NPs (24 nm) and TX-Ag NPs (20 nm) subsequently increased to 32-58 nm with progressive addition of $Au^{3+}$ ions (15-35 μL) signifying the coating of Au on Ag NPs (ESI, Fig. S2a, S3a). In addition, the zeta potential measurements specified that the as-synthesized PVP-Ag NPs (-3.5 mV), CTAB-Ag NPs (+33.02 mV) and TX-Ag NPs (-12.4 mV), were negatively and positively charged confirming the presence of a weakly adsorbed layer of PVP (-6.59 mV), CTAB (+33.45 mV) and TX-100 (-7.6 mV) capping agents, respectively, on their surfaces. However, the deposition of $Au^{3+}$ ions on PVP-Ag NPs led to the increase in magnitude of negative surface charge (-5.6 to -11.9 mV) as shown in Fig. 5b. This charge alteration was probably due to the electron charge donation from Ag with low ionization potential (7.58 eV) to Au with high ionization potential (9.22 eV)[12,43,44] resulting in accumulation of negative charge which was evidenced by XPS measurements and density functional theory in the previous report.[12] Similarly, the net effective charge of bimetallic Ag-Au NCs arising from CTAB-Ag NPs and TX-Ag NPs were also measured to be negative (ESI, Fig. S2b, S3b) as explained above.

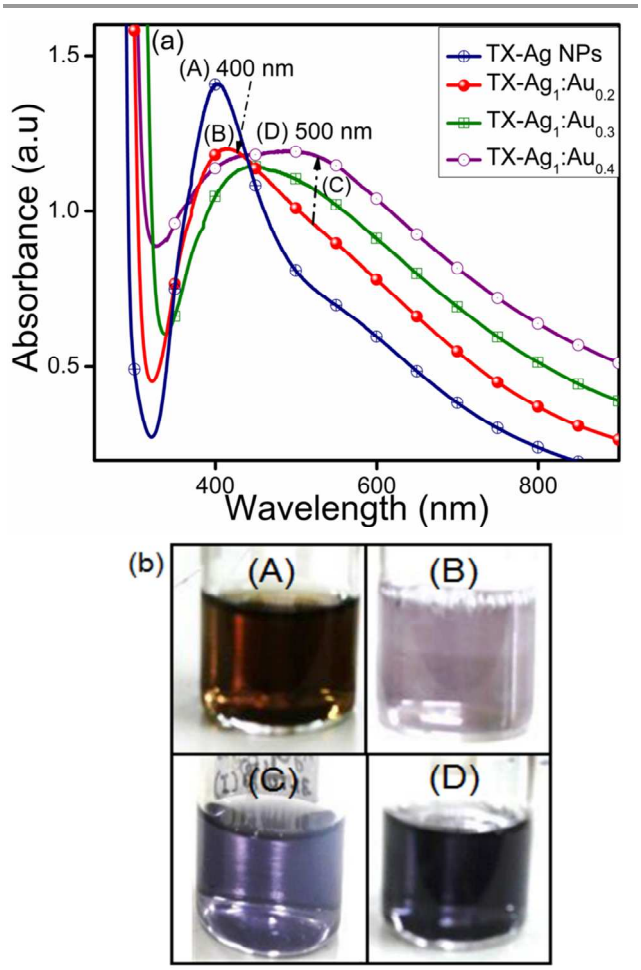


**Fig. 4.** Effect of different amounts (15-35 μL) of $HAuCl_4.3H_2O$ (0.01 M) deposition onto TX-Ag nanoparticles for the (a) variation in the surface plasmon band, and (b) their respective color changes.

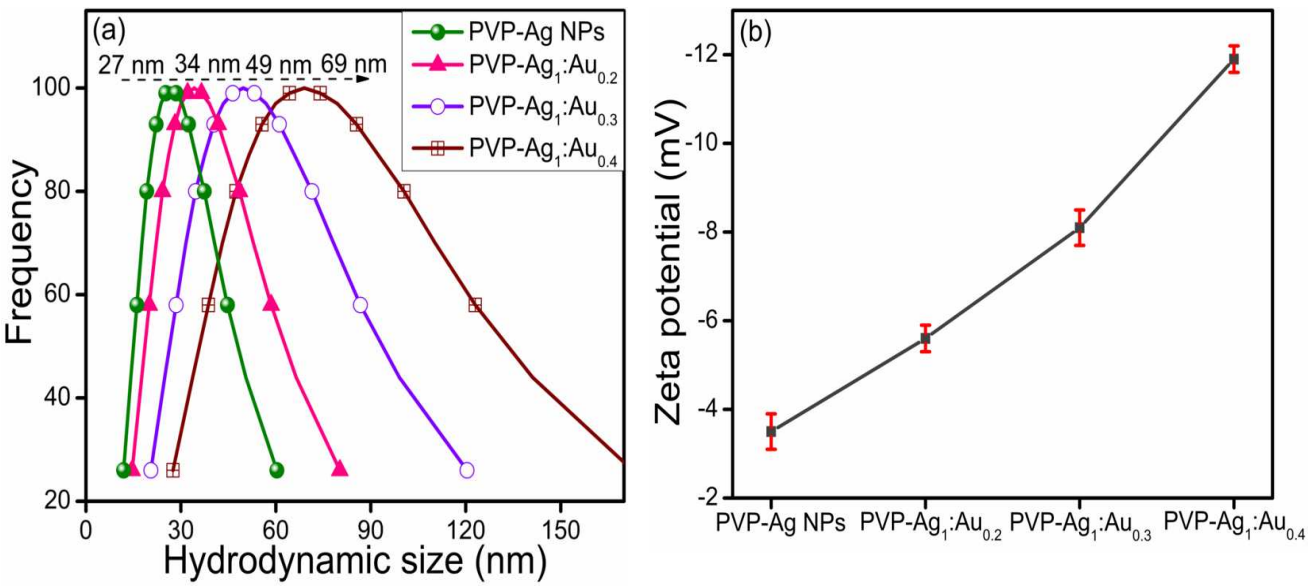


**Fig. 5.** (a) DLS particle size distribution, and (b) Zeta potential of PVP-Ag nanoparticles after deposition of HAuCl4.3H2O (0.01 M) of different amounts (15-35 μL) onto its surface.

### 3.3. Fluorescence properties

The change in the photo-luminescent behavior of Ag NPs after Au coating on its surface was studied by measuring their fluorescence emission spectra (Fig. 6). The emission maximum of PVP-Ag NPs was observed at 305 nm and 600 nm on excitation at 225 nm. The strong emission band at 305 nm can probably be assigned to the Ag–Ag interactions, as reported by other authors.[45,46] However, the weak emission band at 600 nm might be due to the radiationless recombination of the charge species at the surface defect sites. On the addition of $Au^{3+}$ to the surface of PVP-Ag NPs, the fluorescence intensity of pure Ag metal was considerably reduced due to the quenching by Au with an increase in its concentration (Fig. 6), which was similar to an observation made in the earlier report.[47] This effect was due to the blocking of superficial surface traps of the Ag NPs by the thick Au layer formation which strongly evidenced the change in morphology resulting from surface capping of Ag NPs by Au.

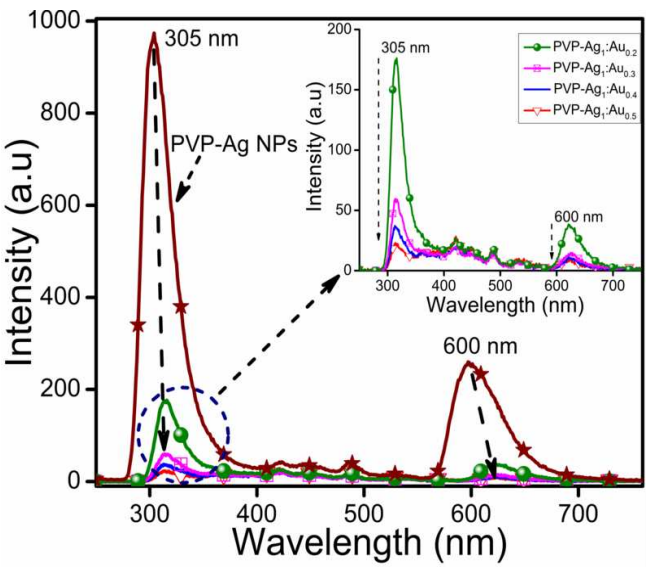


**Fig. 6.** Influence of different amounts (15-35 μL) of HAuCl4.3H2O (0.01 M) deposition on the emission spectra of PVP-Ag nanoparticles (λmax = 225 nm).

### 3.4. Morphological studies

Using the PVP-Ag NPs (~10-11 nm) as the reaction template, the galvanic replacement with Au resulted in the formation of hollow Ag-Au shell (~15 nm) as shown in Fig. 7. With the incoming $Au^{3+}$ ions, the Ag NPs are oxidized into $Ag^{+}$ ions due to the higher reduction potential of $Au^{3+}$/Au (0.99 V) than $Ag^{+}$/Ag (0.80 V).[48] As a result, a galvanically reduced layer of Au atoms formed on the surface of Ag NPs, while oxidized $Ag^{+}$ ions diffused out continuously across the boundaries of the Au-shell during the reaction giving rise to hollow Ag-Au shells with cavity size ~8 nm (Fig. 7b). Further, the SAED pattern of PVP-Ag-Au NCs confirmed the planes (110) and (006) of Ag and (200) and (220) of Au NPs, indicating the presence of both Au and Ag (Fig. 7c) as also reported in the previous literature.[49] On the other hand, CTAB-Ag NPs used as a seed for the deposition of Au furnished mixed solid Ag-Au alloy morphology of size ~20-25 nm rather than hollow shells. Due to the similar lattice constant (2.35 Å for Au and 2.36 Å for Ag), the two metal elements are miscible in all proportions[50,51] and thus, facilitated the alloy formation (Fig. 8 and ESI, Fig. S4). In this context, the TEM images clearly show the dense and light particles corresponding to Au and Ag nanoparticles, respectively, fashioned in non-uniform or irregular manner. In contrast, the porous-hollow aggregates of Ag-Au

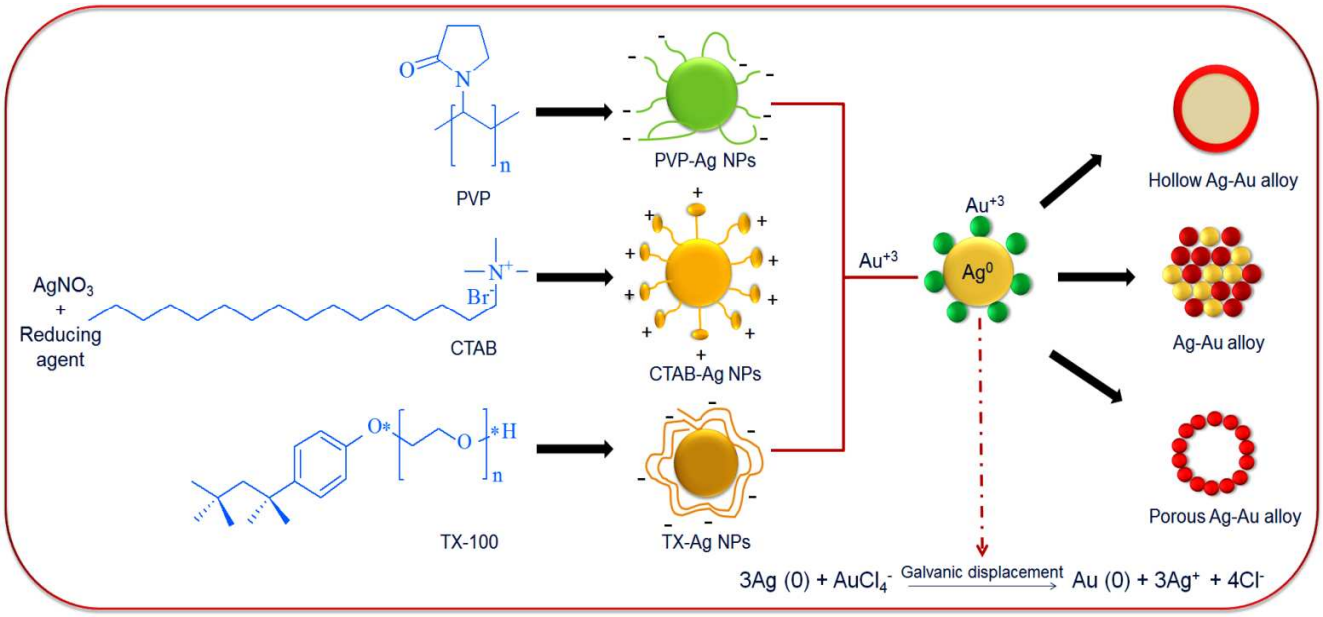


**Scheme 1.** Schematic representation showing the effect of different surfactants capping Ag nanoparticles for the formation Ag-Au bimetallic nanostructures.

nanostructures were evolved after the reaction between $Au^{3+}$ and TX-Ag NPs. The resulting NCs appeared to be composed of a number of smaller metal NPs that are interconnected to form a porous and hollow morphology (size = ~16-22 nm) as seen in Fig. 9 and ESI, Fig. S5. As a result of the displacement reaction, the Au atoms underwent nucleation on the surface of Ag NPs along with the formation of the hole due to the consumption of Ag.[32] This continues until the whole Ag NPs template is etched with $AuCl_4^-$ and subsequently developed into larger bimetallic lobes. In addition, the SAED pattern of porous-hollow Ag-Au aggregates showed the presence of both Au and Ag corresponding to the planes (311) and (103), respectively, as depicted in Fig. 9d.

Therefore, the diverse morphologies of bimetallic NPs were obtained using Ag NPs absorbed with various surfactants of different chemical nature to template the galvanic reaction as evidenced by UV-Vis absorption studies and TEM images. This can be attributed to the difference in reaction rates between the $Au^{3+}$ ions and the surfactants passivizing the Ag NPs surface and hence altering the galvanic Au deposition rate. The strong electrostatic interaction between the PVP/ TX-Ag NPs and the incoming $Au^{3+}$ ions promotes faster Au deposition and thereby displacing the Ag atoms from its core, which resulted in the formation of hollow spaces in contrast to CTAB-Ag NPs as seen in Scheme 1.

### 3.5. Catalytic activity

The comparative catalytic activity of Ag NPs as well as Ag-Au bimetallic NCs was investigated for the reduction of chloro-nitrobenzene (CNB) to chloro-aminobenzene (CAB) by $NaBH_4$ as shown in the scheme of Fig. 10. The absorption spectra for the reduction of CNB (265 nm) by $NaBH_4$ exhibited insignificant changes in the absence of Ag NPs up to 120 min (ESI, Fig. S6a). However, with the addition of Ag NPs, the reaction rate was accelerated and the absorption band intensity

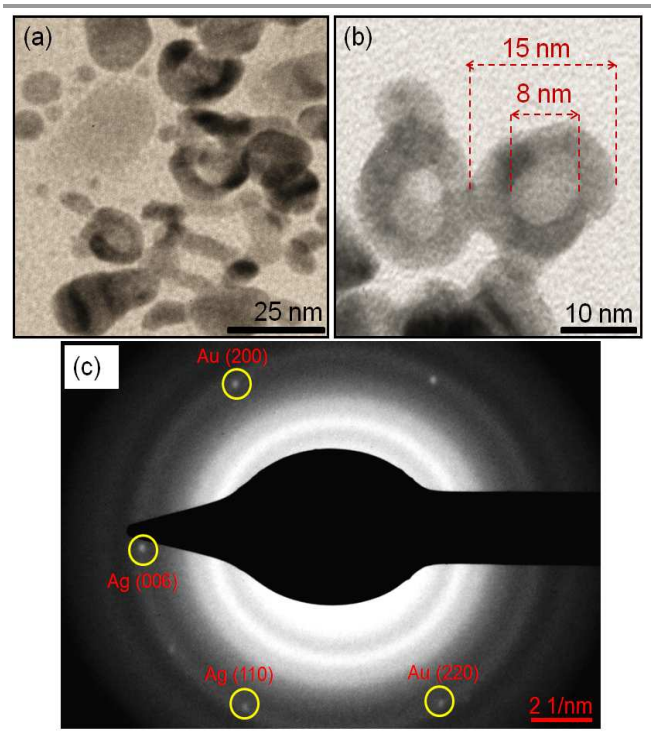


**Fig. 7.** (a-b) TEM images of Au deposited PVP-Ag nanoparticles, and (c) SAED pattern obtained from image (b).

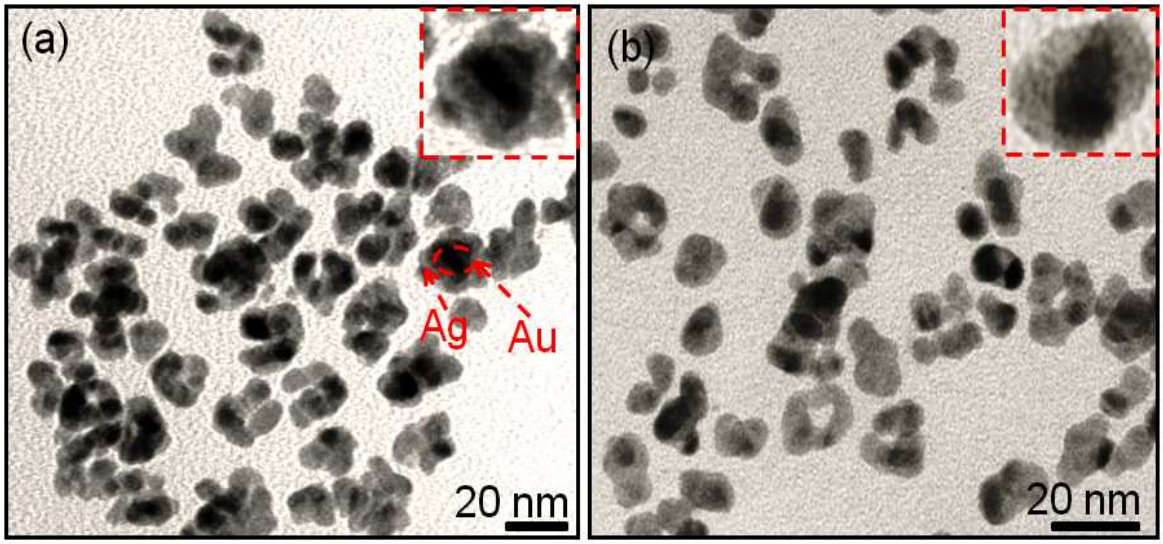


**Fig. 8.** TEM images of Au deposited CTAB-Ag nanoparticles.

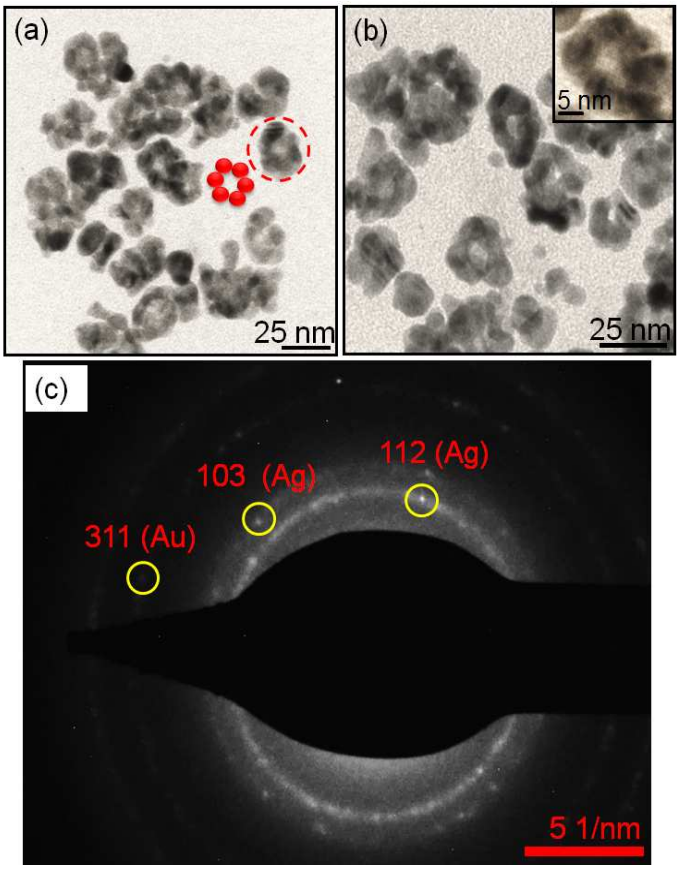


**Fig. 9.** TEM images of Au deposited TX-100 Ag nanoparticles, and (c) SAED pattern obtained from image (b).

corresponding to CNB at 265 nm was gradually reduced and a new absorption band evolved at 280 nm for the formation of CAB (ESI, Fig. S6b). The time course studies (Fig. 10a) displayed that PVP-$Ag_1$:$Au_{0.2}$ NCs exhibited the higher reduction of CNB, (concentration left = ~37%) with higher yield of CAB (71%) within 60 min as compared to monometallic PVP-Ag NPs (63%, within 70 min) as depicted in Fig. 10b. With the growing atomic ratio of Au (0.3 to 0.4) on PVP-Ag NPs, the progressive increase in CAB yield (83-93%) within 50-55 min was observed in Fig. 10b. This is due to the fact that the increasing percentages of Au atoms have a critical effect on the morphology of Ag NPs which resulted in the formation of hollow Ag-Au bimetallic NCs dictating major influence on the catalytic activity. The hollow Ag-Au alloy could possess larger surface areas, reduced densities and the inner surface of the hollow shell may provide more bonding sites for the chemical reaction exhibiting higher catalytic performances.[52-54] From Fig. 10c-d, the CTAB capped $Ag_1$-$Au_{0.3}$ alloy bimetallic NCs showed higher yield (77%, 45 min) for the CAB formation as compared to bare CTAB-Ag NPs (54%, 75 min). The superior catalytic activity can be related to the Ag/Au interface undergoing electronic effect, where Ag has a lower work function than Au.[55] Therefore, electron transfer takes place from Ag to Au near an Ag/Au interface. This ends up with an electron enriched region inside the Au, facilitating the uptake of electrons by adsorbed CNB molecules on the surface of such region. However, further increase in the Au atomic ratio (0.4) on CTAB-Ag NPs comparatively decreases the product yield to 60% within 65 min reduction time. This can be ascribed to the decrease in accessible interfaces, as the increased addition of Au might start covering the Ag/Au interface which makes them inaccessible for the efficient electronic effect. Similarly, the hollow porous aggregates of Ag-Au alloy evolved from the galvanic replacement reaction between the TX-Ag NPs and varying atomic ratio of $Au^{3+}$ ions

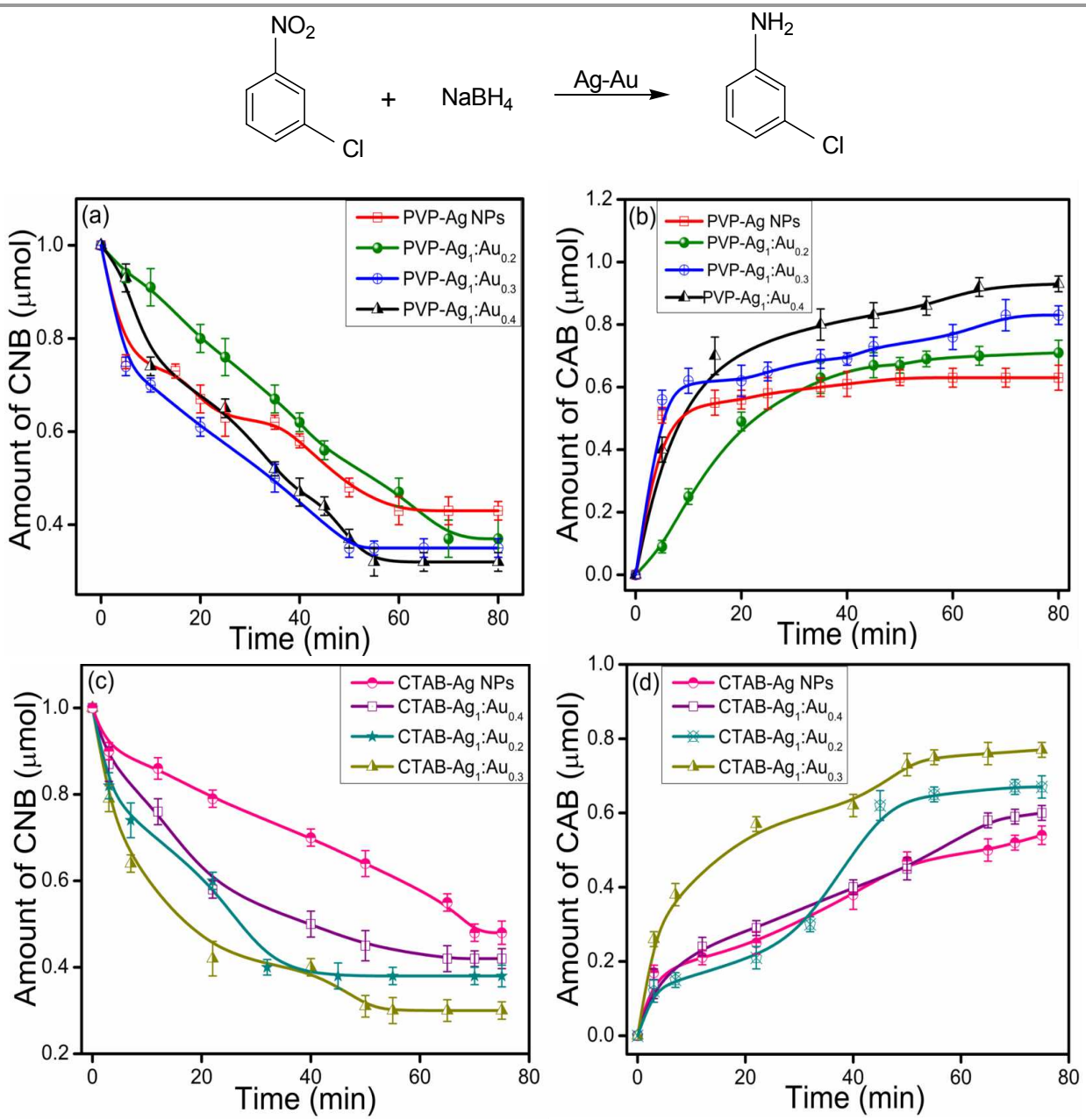


**Fig. 10.** Time course graph for the catalytic reduction of 2-chloro-3-nitrobenzene to 2-chloro-3-aminobenzene by mono and bimetallic (a-b) PVP-Ag nanoparticles, and (c-d) CTAB-Ag nanoparticles.

(0.2 to 0.4) displayed better catalytic performances (57-80%) than monometallic TX-Ag NPs (23%) as shown in ESI, Fig. S7. The porosity in a frame-structured Ag-Au nanostructure might have larger surface areas (both inner and outer) and an improved electrical connection between NPs[31] to accommodate the higher reduction of CNB.

The different Ag-Au bimetallic nanostructures obtained from variously capped Ag NPs with a particular Au atomic ratio exhibited highest catalytic performances as discussed above and was further used as a catalyst for the reduction of nitrobenzene (NB) and nitrotoluene (NT) as shown in Fig. 11. The reproducibility tests were judged by another set of experiments carried out under similar condition as demonstrated in ESI, Fig. S8 and Section S9. Overall, the different bimetallic nanocatalyst can be ordered as follows, PVP-$Ag_1$:$Au_{0.4}$ > TX-$Ag_1$:$Au_{0.4}$ > CTAB-$Ag_1$:$Au_{0.3}$ attributed to their respective morphology. Among NB, CNB and NT, the compound with an electron withdrawing group ($–Cl^-$) reflects higher catalytic activity relative to the compound with electron-donating group ($–CH_3$), as can be seen in Fig. 11. The higher inductive (+0.34) and lower resonance stabilization value (-0.07) of chloro group relative to low inductive (-0.04) and high stabilization parameters (-0.11) of methyl group reflected faster rate of reduction for chloro group.[56] Hence, the conversion of



 

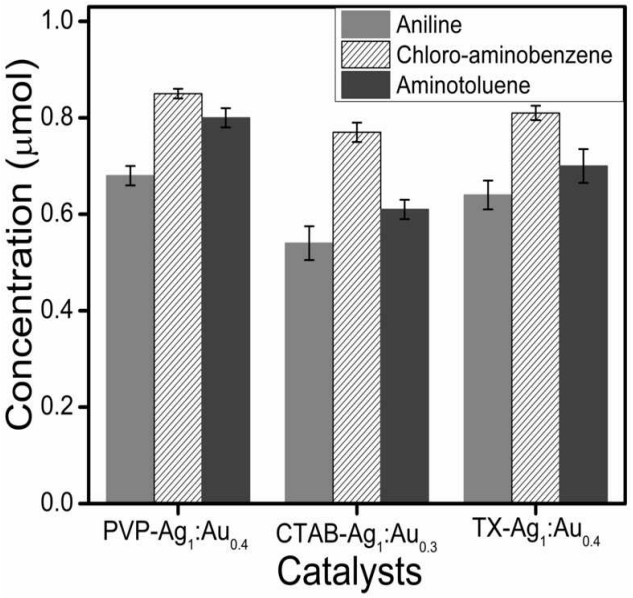


**Fig. 11.** Amount of aniline, chloro-aminobenzene and aminotoluene produced during reduction of nitrobenzene, 2-chloro-3-nitrobenzene and nitrotoluene by different Ag-Au bimetallic nanostructures, respectively.

nitro-aromatic compounds to their respective products were seen to be enhanced by bimetallic NCs as compared to their monometallic counterparts. Therefore, through the optimization of the composition of these two metals (Ag and Au), the catalytic efficiency can be improved for the purpose of other reduction processes.

## 4. Conclusions

In summary, a simple technique has been demonstrated to control the morphology of Ag-Au bimetallic nanocomposites using Ag template capped with surfactants of different chemical nature. A significant variation in the optical properties of Ag NPs can be obtained at a desired level as a function of concentration of Au, which is essential for the application in surface-enhanced Raman spectroscopy (SERS) and optical sensing. Upon reaction with $AuCl_4^-$ ions, the Ag NPs templates are converted either to solid, hollow or porous Au-Ag alloy NPs depending on the adsorbed surfactants on the Ag NPs surface. This ability to tailor NPs morphology and surface composition allows the systematic studies of the synergistic role of Au and Ag, and the evaluation of these bimetallic as potential nanocatalysts for various organic syntheses.

## Acknowledgements

We acknowledge Dr. B. N. Chudasama (School of Physics and Material Science, Thapar University) for Zeta potential and DLS measurement. sWe would also like to thank to Sophisticated Analytical Instrumentation Facility (IIT Bombay) for TEM analysis. We acknowledge CSIR for the financial support.

## Notes and references

School of Chemistry and Biochemistry, Thapar University, Patiala-147004, Punjab, India.
E-mail: bpal@thapar.edu.
Fax: +91-175-236-4498; Tel: +91-175-239-3491.

Electronic Supplementary Information (ESI) available: Calculations of Ag/Au atomic ratio, Electrokinetic parameters of monometallic CTAB-Ag NPs, TX-Ag NPs and their respective Ag-Au bimetallic NCs, TEM images of different Ag-Au bimetallic NCs, UV-Vis absorption spectra for the reduction of chloronitrobenzene to chloroaminobenzene, Time course graph showing catalytic activity of monometallic TX-Ag NPs and their Ag-Au bimetallic NCs and HPLC chromatograms. See DOI: 10.1039/b000000x/

1 A. Roucoux, J. Schulz and H. Patin, *Chem. Rev.*, 2002, **102**, 3757.
2 M. Moreno-Manas and R. Pleixats, *Acc. Chem. Res.*, 2003, **36**, 638.
3 Y. Zhang, X. Cui, F. Shi and Y. Deng, *Chem. Rev.*, 2012, **112**, 2467.
4 Y. Mikami, A. Dhakshinamoorthy, M. Alvaro and H. Garcia, *Catal. Sci. Technol.*, 2013, **3**, 58.
5 Y. Cui, B. Ren, J. L. Yao, R. A. Gu and Z. Q. Tian, *J. Phys. Chem. B*, 2006, **110**, 4002.
6 R. G. Freeman, M. B. Hommer, K. C. Grabar, M. A. Jackson and M. J. Natan, *J. Phys. Chem.*, 1996, **100**, 718.
7 N. R. Jana, *Analyst*, 2003, **128**, 954.
8 Y. W. Cao, R. Jin and C. A Mirkin, *J. Am. Chem. Soc.*, 2001, **123,** 7961.
9 Y. Yang, J. Liu, Z.W. Fu and D. Qin, *J. Am. Chem. Soc.*, 2014, **136**, 8153.
10 L. Lu, A. Kobayashi, K. Tawa and Y. Ozaki, *Chem. Mater.*, 2006, **18**, 4894.
11 C. Shankar, A. T. N. Dao, P. Singh, K. Higashimine, D. M. Mott and S. Maenosono, *Nanotechnology*, 2012, **23**, 245704.
12 S. Nishimura, A. T. N. Dao, D. Mott, K. Ebitani and S. Maenosono, *J. Phys. Chem. C*, 2012, **116**, 4511.
13 Y. Ju-Nam and J. R. Lead, *Sci. Total Environ.*, 2008, **400**, 396.
14 M. E. Badawy, T. P. Luxton, R. G. Silva, K. G. Scheckel, M. T. Suidan, and T. M. Tolaymat, *Environ. Sci. Technol.*, 2010, **44**, 1260.
15 D. T. N. Anh, P. Singh, C. Shankar, D. Mott and S. Maenosono, *Appl. Phys. Lett.*, 2011, **99**, 073107.
16 D. Mott, N. T. B. Thuy, Y. Aoki and S. Maenosono, *Phil. Trans. R. Soc. A*, 2010, **368**, 4275.
17 N. Toshima and T. Yonezawa, *New J. Chem.*, 1998, **22**, 1179.
18 D. S. Wang and Y. D. Li, *Adv. Mater.*, 2011, **23**, 1044.
19 H. L. Jiang and Q. Xu, *J. Mater. Chem.*, 2011, **21**, 13705.
20 R. Ferrando, J. Jellinek and R. L. Johnston, *Chem. Rev.*, 2008, **108**, 845.
21 A. Monga and B. Pal, *New J. Chem.*, 2015, **39**, 304.
22 X. Zhang and Z. Su, *Adv. Mater.*, 2012, **24**, 4574.
23 B. E. Brinson, J. B. Lassiter, C. S. Levin, R. Bardhan, N. Mirin and N. J. Halas, *Langmuir*, 2008, **24**, 14166.
24 Y. Xiang, X. Wu, D. Liu, Z. Li, W. Chu, L. Feng, K. Zhang, W. Zhou and S. Xie, *Langmuir*, 2008, **24**, 3465.
25 H. F. Zarick, W. R. Erwin, J. Aufrecht, A. Coppola, B. R. Rogers, C. L. Pint and R. J. Bardhan, *Mater. Chem. A*, 2014, **2**, 7088.

26 N. R. Sieb, N. C. Wu, E. Majidi, R. Kukreja, N. R. Branda and B. D. Gates, *ACS Nano*, 2009, **3**, 1365.
27 L. Han-Pu, W. Li-Jun, B. Chun-Li and J. Li, *J. Phys. Chem. B*, 2005, **109**, 7795.
28 A. M. Schwartzberg, T. Y. Olson, C. E. Talley and J. Z. Zhang, *J. Phys. Chem. B*, 2006, **110**, 19935.
29 Y. D. Yin, R. M. Rioux, C. K. Erdonmez, S. Hughes, G. A. Somorjai and A. P. Alivisatos, *Science*, 2004, **304**, 711.
30 S. E. Skrabalak, J. Chen, L. Au, X. Lu, X. Li and Y. Xia, *Adv. Mater.*, 2007, **19**, 3177.
31 J. Zeng, Q. Zhang, J. Chen and Y. Xia, *Nano Lett.*, 2010, **10**, 30.
32 S. W. Hsu, K. On, B. Gao and A. R. Tao, *Langmuir*, 2011, **27**, 8494.
33 J. H. Liu, A. Q. Wang, Y. S. Chi, H. P. Lin, C. Y. Mou, *J. Phys. Chem. B*, 2005, **109**, 40.
34 N. R. Jana, L. Gearheart and C. J. Murphy, *Langmuir*, 2001, **17**, 6782.
35 G. Kawamura, Y. Yang, and M. Nogami, *J. Phys. Chem. C*, 2008, **112**, 10632.
36 P. Y. Silvert, R. H. Urbina and K. Tekaia-Elhsissena, *J. Mater. Chem.*, 1997, **7**, 293.
37 Y. Yang, S. Matsubara, L. Xiong, T. Hayakawa and M. Nogami, *J. Phys. Chem. C*, 2007, **111**, 9095.
38 B. Rodriguez-Gonzalez, A. Burrows, M. Watanabe, C. J. Kiely and L. M. L. Marzan, *J. Mater. Chem.*, 2005, **15**, 1755.
39 M. Liu and P. Guyot-Sionnest, *J. Phys. Chem. B*, 2004, **108**, 5882.
40 S. Eustis and M. A. El-Sayed *Chem. Soc. Rev.,* 2006, **35**, 209.

41 I. Ojea-Jimenez and V. Puntes, *J. Am. Chem. Soc.*, 2009, **131**, 13320.
42 M. Kahraman, O. Aydin and M. Culha, *Plasmonics*, 2009, **4**, 293.
43 H. Zhanga and N. Toshima, *Catal. Sci. Technol.*, 2013, **3**, 268.
44 S. Tokonami, N. Morita, K. Takasaki and N. Toshima, *J. Phys. Chem. C*, 2010, **114**, 10336.
45 F. X. Xie, H. Y. Bie, L. M. Duan, G. H. Li, X. Zhang and J. Q. Xu, *J. Solid State Chem.*, 2005, **178**, 2858.
46 A. Zhanga, J. Zhanga and Y. Fang, *J. Lumin.*, 2008, **128**, 1635.
47 M. Ganguly, A. Pal, Y. Negishi and T. Pal, *Langmuir*, 2013, **29**, 2033.
48 Y. Choi, S. Hong, L. Liu, S. K. Kim and S. Park, *Langmuir*, 2012, **28**, 6670.
49 T. Ghosh, B. Satpati and D. Senapati, *J. Mater. Chem. C*, 2014, **2**, 2439.
50 Z. Peng, B. Spliethoff, B. Tesche, T. Walther and K. Kleinermanns, *J. Phys. Chem. B*, 2006, **110**, 2549.
51 S. Liu, G. Chen, P. N. Prasad and M. T. Swihart, *Chem. Mater.*, 2011, **23**, 4098.
52 H. Wu, P. Wang, H. He and Y. Jin, *Nano Res.*, 2012, **5**, 135.
53 M. R. Kim, D. K. Lee and D. Jang, *J. Appl. Catal. B*, 2011, **103**, 253.
54 H. M. Chen, R. S. Liu, M. Y. Lo, S. C. Chang, L. D. Tsai, Y. M. Peng and J. F. Lee, *J. Phys. Chem. C*, 2008, **112**, 7522.
55 J. Huang, S. Vongehr, S. Tang, H. Lu, J. Shen and X. Meng, *Langmuir*, 2009, **25**, 11890.
56 C. Bougheloum and A. Messalhi, *Phys. Procedia,* 2009, **10**, 1055.



 